Investigations on Sonic Normal and Oblique Jets in Hypersonic Cross-Flow

Ratan Joarder, G. Jagadeesh

Department of Aerospace Engineering, Indian Institute of Science, Bangalore, India

Abstract

This paper presents the results of numerical and experimental investigations on sonic jet (nitrogen) injections into a hypersonic cross-flow of air. The simulations aim at finding suitable injection conditions consistent with the experimental facility at IISc from the viewpoint of combustion. Numerical results under predicted the measured jet penetration depth for normal injection. It is found from numerical simulations that the total pressure loss in case of oblique injection is less than the normal injection.

1. INTRODUCTION

Recently there is a resurgence of interest in SCRAMJET (supersonic combustion ramjet) engines. People are trying different methods to achieve combustion at supersonic speeds in different parts of the world. Combustion at supersonic speeds needs techniques for enhancement of fuel and oxidizer mixing as well as reduction of ignition-delay lengths [1]. Additionally total pressure loss and increase of wave-drag due to shocks arising as a consequence of injection of fuel into the oncoming supersonic stream sets a challenge in designing practical SCRAMJET engines. In other words, engine generated thrust needs to overcome the wave drag and frictional drag on the body efficiently.

Traditionally numerical simulations and experiments are carried out by different groups of people. If the sole purpose is to validate experimental results numerically or vice versa, the approach works. In the present case the necessity of developing a system right from the scratch has forced to deal with the two things by a single group. Different experimental conditions in the facility from the data available in the literature and the necessity to tune the conditions also added to the cause.

The simplest method of fuel delivery into the combustion chamber is, perhaps, injection from the wall of the combustion chamber. Although the physicochemical properties of the system(mixture of air and fuel) is going to vary in presence or absence of generation of heat, in the preliminary stage of development a case without heat release is considered. In other words, a non-reacting gas (nitrogen) is injected into a hypersonic cross-flow of air and the resulting flow field is studied. The experimental facility at IISc provides a free-stream Mach number of 5.75. Although it is possible to reduce the Mach number at the entrance of the observation region to 2, which is more practical from the point of view of combustion, in the present case it is not tried. The results may extend the existing literature on jet injection into supersonic cross-flows. Additionally, the results could be used in a recent concept on SCRAMJETs called "Radical farming" [1] in which a fuel is injected from inlet wall where the flow is high supersonic or hypersonic. The inlet reduces the Mach number of oncoming air to low supersonic values accompanied by rise in pressure.

Injection from inlet increases the length which the fuel has to mix with oncoming air. Traditionally fuel is delivered into the combustion chamber either from walls or through strut-injection [2].

In earlier times when numerical simulations of a complete three dimensional case was not possible because of absence of numerical schemes and limited computer resources, prediction of jet penetration were made by analytical expressions which required inputs from experiments [3, 4]. Additionally, various simplifying assumptions were also present, e.g. no mixing of jet and the cross-flow, treatment

of jet as a solid body obstructing the flow. In some cases power law fit of the jet trajectory were also made based on experimental observations.

The earliest report on experiments in slot injection (injection through a slot across the span of a flat plate) is by Spaid and Zukoski [5]. The experiments are conducted for a range of supersonic speeds (M_∞ = 2.61, 3.50 and 4.54) with a very narrow slot width (0.2668 mm) on a flat plate. The experiments by Aso et al. [6] report wall injection results for pressure distributions and flow patterns on the wall through oil flow visualization. Qualitative studies of flow features using PLIF and Mie scattering by Gruber et al. [7], quantitative velocity and turbulent field data using LDV by Santiago and Dutton [8] and wall pressure distribution using pressure sensitive paint by Everett et al. [9] are also reported. With the advent of ultra fast cameras, it is possible to study evolution of flow field structure for very small time intervals. Ben-Yakar et al. [10] reports the evolution of vortical structure of hydrogen and ethylene transverse jets in a supersonic cross-flow experimentally. With a very high speed camera, they are able to track eddies at 1 microsecond interval. Mixing and penetration are found to be more for ethylene than hydrogen jets. Rizzetta [11] used an unsplit finite difference Mac-Cormack scheme and the k-ε model to simulate experiments of Aso et al. [12]. Grasso and Magi [13] simulate hydrogen and helium injection using Roe's scheme and the k–ε model, and find good agreement with experimental wall pressure data. Gerlinger et al. [14] use an implicit lower-upper symmetric Gauss-Siedal method and solve the k–ε model in an uncoupled manner. They test the code with few experiments of Aso et al. [12] and observe no notable effect of compressibility correction on wall pressure predictions. Dhinagaran and Bose [15] use a time split, finite volume Mac-Cormack method with Baldwin-Lomax model and simulate experiments of Spaid and Zukoski [5]. For higher injection pressure ratio, applying a relaxation on the eddy viscosity improve upstream prediction.

The objective of the present study was to numerically determine suitable jet injection conditions consistent with experimental conditions available at the IISc hypersonic shock tunnel HST2. The conditions should produce a reasonable jet penetration (experimentally) into the oncoming hypersonic cross-flow efficiently from the viewpoint of combustion. Determination of the triggering of injection (the method and time advance) was also one of the objectives in view of the fact that the typical test time was approximately 1 millisecond.

2. NUMERICAL STUDIES
2.1 Governing equations and finite volume formulation
The Navier-Stokes equations with k–ε turbulence model [16] in vector integral conservation-law form may be expressed as

$$\frac{\partial}{\partial t}\iiint \boldsymbol{U}dv + \iint (\boldsymbol{\mathcal{H}} - \boldsymbol{\mathcal{F}}).\boldsymbol{\hat{n}}ds = \iiint \boldsymbol{S}\,dv \qquad (1)$$

Complete description of each term of equation 1 can be found in Ratan et al. [17]. In short $\boldsymbol{U}$ and $\boldsymbol{S}$ are column vectors containing conservative variables and source terms respectively, $\boldsymbol{\mathcal{H}}$ and $\boldsymbol{\mathcal{F}}$ are second order flux tensors containing inviscid and viscous fluxes respectively. $\mathbf{U} = [\rho, \rho u, \rho v, \rho w, \rho E, \rho k, \rho \omega]^T$ where ρ, u, v, w, k, ω and E represent density, x, y, z, component of velocity, turbulence kinetic energy, specific dissipation rate and total internal energy respectively. The equations are non-dimensionalized by a length scale (length of the domain under consideration, l), a velocity scale (free-stream sound speed, a_∞), a density scale (free-stream density, ρ_∞) and free-stream viscosity (μ_∞) in all computations. A suitable computational domain is chosen depending on the requirement. The computational domain is divided into finite volumes. Without loss of generality, a finite volume V of fluid may be specified as a six-sided boxlike solid and value of dependent variables may be assigned to cell-center of each cell.

2.2 Discretization of fluxes and source terms
The inviscid fluxes are discretized using the approximate Riemann solver of Roe [18]. The eigenvalues, eigenvectors and wave strengths for determining inter-cell fluxes using Roe's scheme with the k-ω

turbulence model may be found in Ratan et al. [17]. To increase the spatial accuracy, a MUSCL extrapolation strategy [19] is followed with Van Albada limiter [20] to suppress spurious oscillations near a strong discontinuity. Viscous fluxes are discretized by central differencing [21] with k-ω model [16] to account for the Reynolds stress terms. Explicit compressibility modeling is done to account for compressibility effects [22] in the shear layer. The source terms are treated implicitly following the method given in Thomas et al. [23].

2.3 Steady-state time integration technique

For each finite volume, the surface integral over S of equation 1 can be written as

$$\iint (\mathcal{H} - \mathcal{F}) . \hat{\boldsymbol{n}} ds = \sum_{i=1}^{6} \iint (\mathcal{H} - \mathcal{F}) . d\boldsymbol{s} \tag{2}$$

where d$\boldsymbol{s}$ represents a differential area of face of a hexahedron. The update formula for conservative variables in a single time stage Δt is given by

$$\boldsymbol{U}^{n+1} = \boldsymbol{U}^n - \frac{\Delta t}{V} \sum_{i=1}^{6} \iint (\mathcal{H} - \mathcal{F}) . d\boldsymbol{s} + \frac{\boldsymbol{S}\Delta t}{1 - \frac{\partial \boldsymbol{S}}{\partial \boldsymbol{U}} \Delta t} \tag{3}$$

For any computational cell it is convenient to write equation 3 as

$$\frac{\partial \boldsymbol{U}}{\partial t} = R(\boldsymbol{U}) \tag{4}$$

The time integration of equation 4 to steady state is carried out based on an explicit multi-stage Runge-Kutta method [24] (instead of a single stage as defined in equation 3) which comprises of the sequence

$$\boldsymbol{U}^{(0)} = \boldsymbol{U}^n$$
$$\boldsymbol{U}^{(k)} = \boldsymbol{U}^{(0)} + \alpha_k R\big(\boldsymbol{U}^{(k-1)}, \Delta t\big), k = 1 \dots m \tag{5}$$
$$\boldsymbol{U}^{(n+1)} = \boldsymbol{U}^m$$

where m denotes number of stages. Values of α_k for a six stage third order accurate integration are [0.0742 0.1393 0.2198 0.3302 0.5181 1.000].

2.4. Grid, boundary conditions, grid sensitivity and numerical results

The flow domain is flow over a flat plate. To reduce CPU time, the domain is restricted to seventeen jet diameters (D) along the flow direction, eight and half jet diameters along the span and height. The domain is discretized by Cartesian hexahedral cells. The height of cells normal to the plate is gradually increased or stretched [25] from the plate to capture the three layers of a wall bounded turbulent flow. Quantitatively it is ensured that the mesh point (cell center) closest to the wall lies below $y^+ = 1$ and that at least 5 mesh points lie between $y^+ = 0$ and $y^+ = 2.5$ [16]. Grid is clustered around the injection points (both span-wise and along flow direction) to capture the region accurately. Figure 1 shows an isometric view of the grid used in the present computations.

The following approximation is made in representing the circular port on a Cartesian grid. The non-dimensional jet radius(r) is found and the number of grid points to represent r is determined. It should

be noted here that the total number of grid points in each direction is given in the next paragraph. Then the numbers of points along stream-wise direction (flow direction), starting from index of center of the port, which fall within rcos ϕ are determined for a fixed value of z. The process is repeated for all z within r. Here cos $\phi = \Delta z/r$. For example, in figure 2, approximately 5 points are necessary to represent half of the port's second row, which is parallel to the stream-wise direction, from the center of the port. In case of the port's fourth row (parallel to the stream-wise direction) approximately 4 points are necessary to represent half of the row from the center of the port. For elliptic port instead of rcos ϕ, it is rcos ϕ/cos 45° because the jet makes 45° with the free-stream direction. The injection conditions are specified on these points starting from index of center of the port in all four quadrants. The free-stream and jet conditions are given in table 1 and 2 respectively. Figure 2 shows a plan view of the Cartesian grid around the circular port.
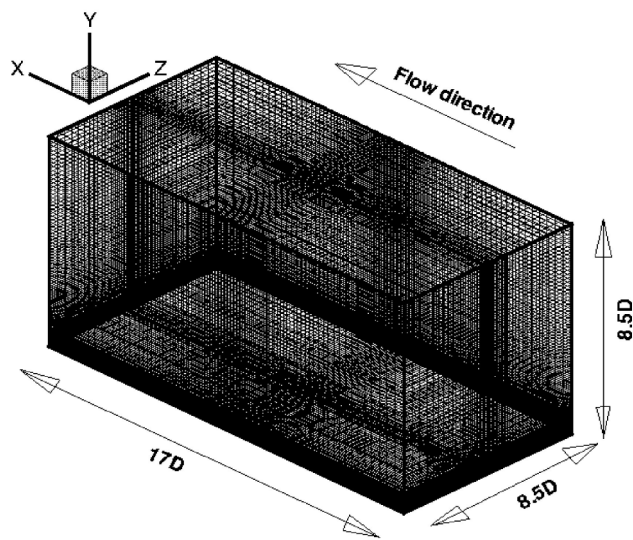
Figure 1.   Isometric view of the grid used the present computations
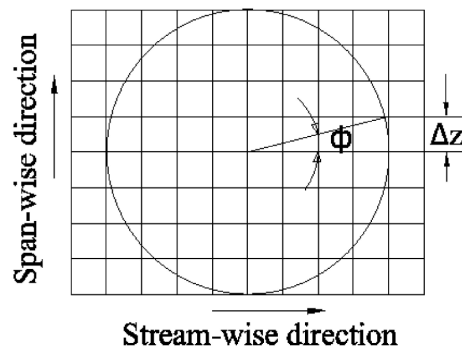
Figure 2.   Plan view of the grid around circular port

The initial and boundary values of pressure, temperature and velocity used in the numerical simulations were determined from experiments which are described later. All dependent variables are specified at the inlet. The free-stream turbulence kinetic energy (k_∞) follows from assuming the free-stream turbulence level $T_{u, \infty} = (2/3 \, k_\infty)^{1/2}/u_\infty$ to be 0.005 [11]. This is one order of magnitude less than the value taken in [26], which possibly talks about an impulse facility. It is sometimes said that the noise

levels in shock tunnels may be lower than in conventional hypersonic wind tunnels [27]. In view of sparse presence of direct measurement of fluctuation levels in shock tunnels, this value is taken for granted. The value of specific dissipation rate ω_∞ is calculated by equating molecular and eddy viscosities. At top, left, and right boundaries and at outlet, all variables are extrapolated from the interior. The lower boundary is a no slip wall except at the injection points. No slip conditions are applied after three grid points from the leading edge. Pressure is extrapolated from the interior. Turbulence kinetic energy is set to zero and the hydraulically-smooth surface condition is used to calculate ω [16]. Jet velocity, static pressure and temperature are specified at the injection points. In case of normal injection, only the component of velocity normal to the wall is specified at injection points whereas for oblique injection, equal wall normal and axial component (free-stream direction) of velocity is specified. Values of k and ω are specified as k_∞ and ω_∞ respectively at the injection points.

The Reynolds number based on length of the domain and free-stream conditions of the experimental facility is 6.36×10^3. The solution is sensitive to the number of grid points and stretching factor. The stretching factor is determined by the Reynolds number for a suitable and fixed number of grid points. A number of simulations are done before arriving at the final number of grid points ($201 \times 101 \times 51$) and stretching factor (1.2) when there is no change in solution nature even if number of grid points is increased. The boundary layer is allowed to develop for around 3000 time steps with CFL number of 0.8. After that the injection is started with a reduced CFL number of 0.05. Simple limiters are used to keep the value of k and ω positive during the initial period of injection. The code is run in parallel mode using the OpenMp model in SGI Altix3700.

Figure 3, 4, 5, 6 show the streamlines for normal and oblique injections for two pressure ratios. For normal injection the port is circular whereas it is elliptic for oblique injection. On the boundary of the domain Mach number contour is shown. The jet has spread larger span-wise for oblique injection than normal injection.
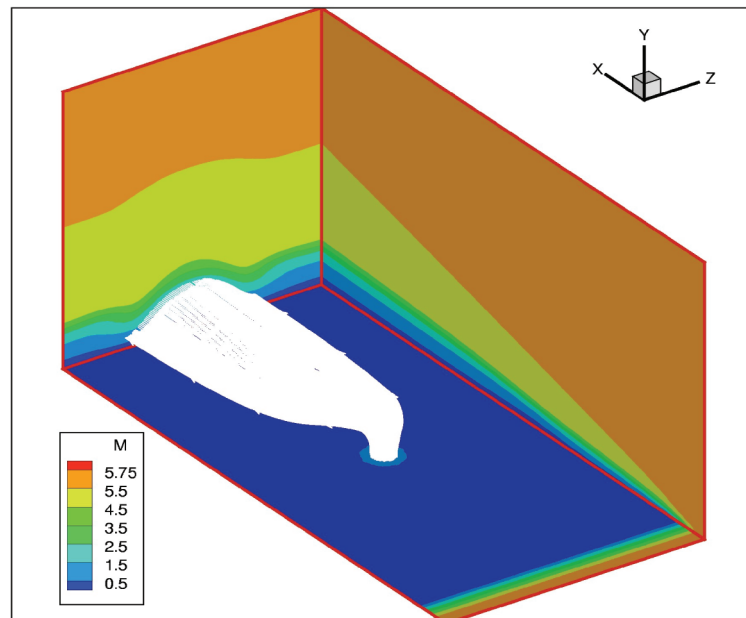
Figure 3.   Isometric view of the domain showing the jet coming out of the circular port along with contour plot of Mach number, Condition 1, normal injection
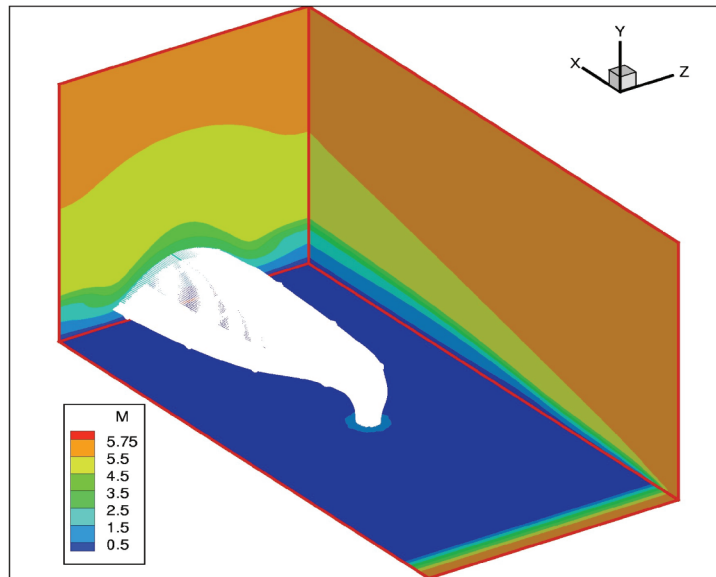
Figure4.   Isometric view of the domain showing the jet coming out of the circular port along with contour plot of Mach number, Condition 2, normal injection
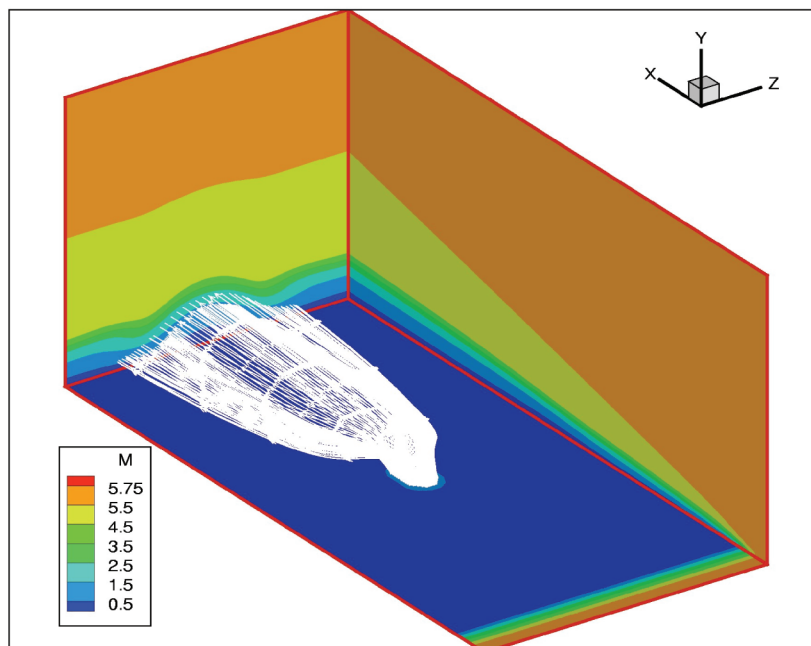
Figure 5.   Isometric view of the domain showing the jet coming out of the elliptic port along with contour plot of Mach number, Condition 1, oblique injection
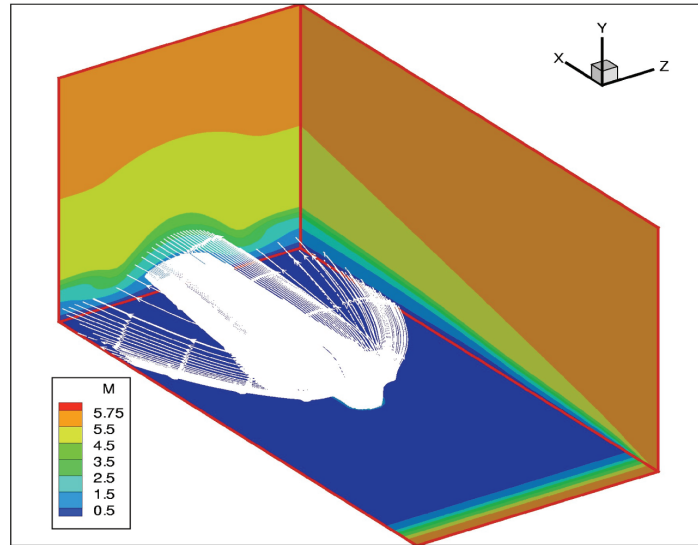
Figure6.   Isometric view of the domain showing the jet coming out of the elliptic port
                 along with contour plot of Mach number, Condition 2, oblique injection

Figures 7 and 8 shows the streamlines which originate from or end on a line passing through the port
center along span-wise direction. The streamlines originating from the inner part of the port penetrates
deeper into the cross-flow than the streamlines originating from outer part of the port. The outermost
streamlines interact with the neighbouring cross-flow streamlines and generates vortices and flow patterns
depending on magnitude and direction of jet velocity. For example, in the normal injection case, the jet
initially does not have a stream-wise component of velocity. Hence the velocity difference in the shear
layer between outer jet and cross-flow creates spiral streamlines (figure 7) in the jet wake. In the oblique
injection case, due to presence of initial stream-wise component of velocity in the jet, the velocity
difference in the shear layer is less than the normal injection case and the spiral streamlines are not
observed in the jet wake. Instead the jet spreads more in the span wise direction. The horse-shoe vortex
is also shown on the bottom wall of figure 7 and 8.
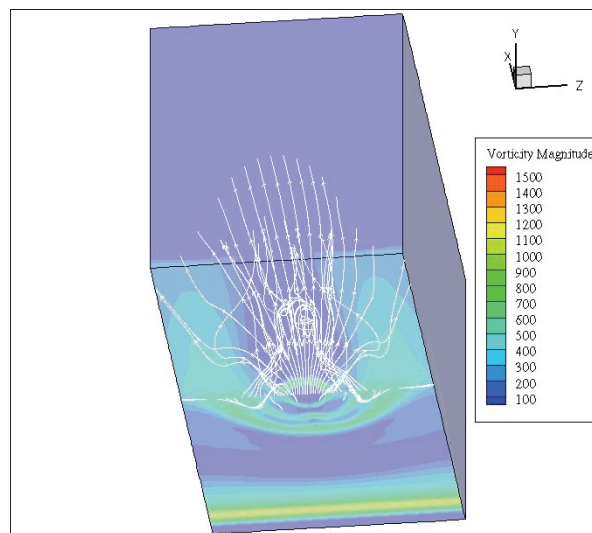
Figure7.   Horse-shoe vortex on the bottom wall along with streamlines originating from
                 or ending on a line passing through the port center in the span-wise direction,
                 condition 1, normal injection, the vorticity magnitude is normalized by l/a_∞, l is
                 the length of the domain
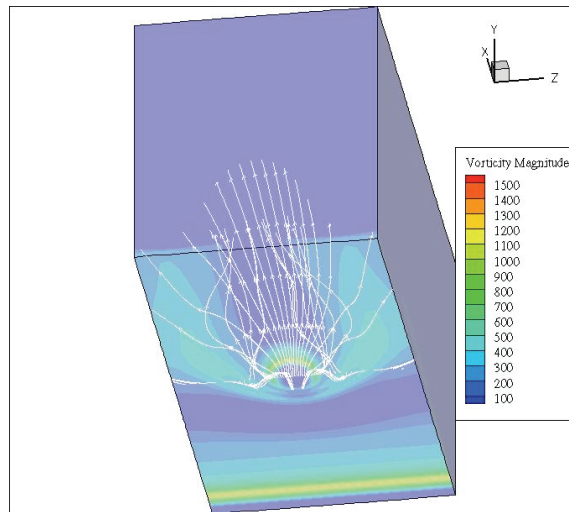
Figure8.   Horse-shoe vortex on the bottom wall along with streamlines originating from or ending on a line passing through the port center in the span-wise direction, condition 2, oblique injection, the vorticity magnitude is normalized by l/a_∞, l is the length of the domain

The penetration depth of the jet into the oncoming free-stream is plotted along with experimental results later. Figure 9 shows plots of the stagnation pressure for normal and oblique injections at inlet and outlet at mid-span of the domain. As can be seen from the figure, the stagnation pressure loss is less for inclined injection. Figure 10 and 11 show the variation of scaled residue

$$\frac{||f^{n+1} - f^n||}{||f^1 - f^0||}$$

with number of iteration. Here f^{n+1} denotes the value of f at $(n + 1)^{th}$ time step and only L_∞ norm is shown. The sharp rise at 3000 iteration is the point when injection is started.
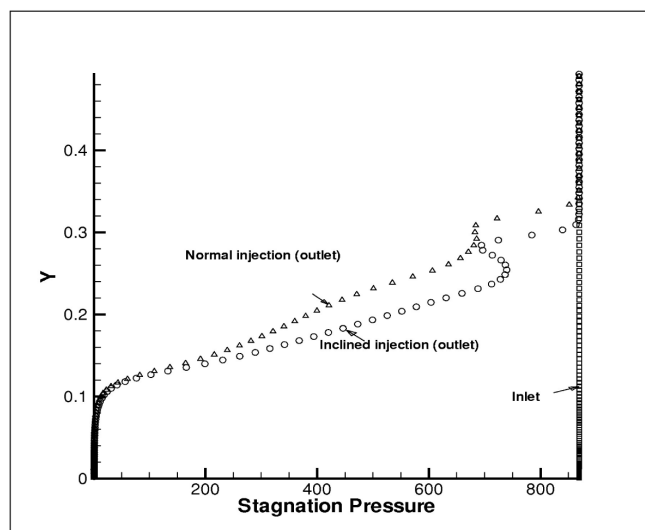
Figure 9.   Stagnation pressure $(p_0/\rho_\infty a_\infty^2)$ distribution at inlet and outlet
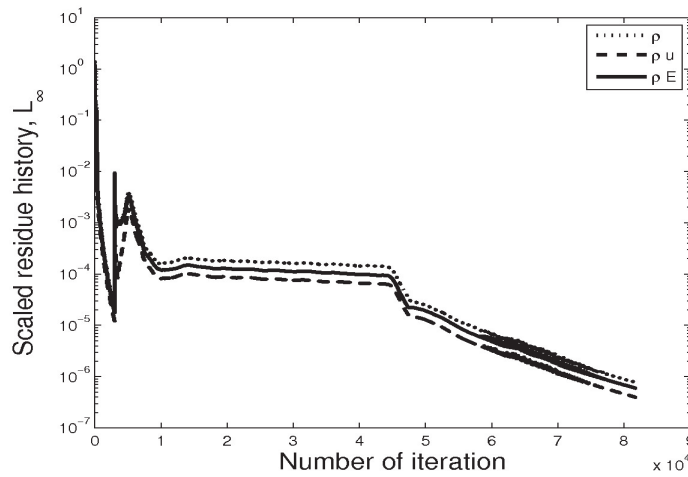
Figure 10.   Scaled residue history for ρ, ρu and ρE
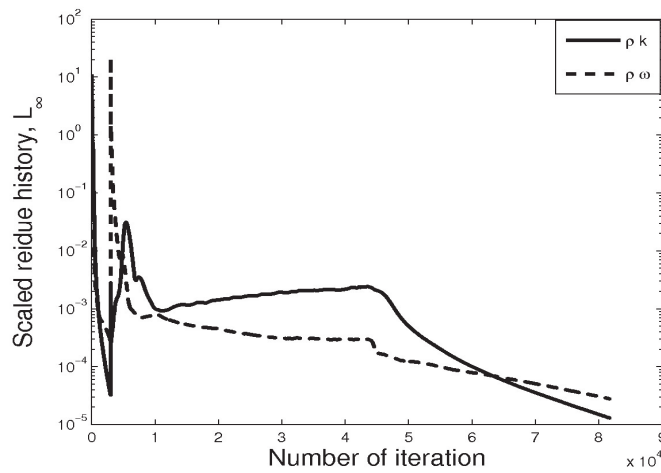
Figure 11.   Scaled residue history for ρk and ρω

3. EXPERIMENTAL SETUP
3.1. IISc Hypersonic Shock tunnel HST2
Experiments were carried out in the IISc hypersonic shock tunnel HST2. Stagnation enthalpies up to 3 MJ/ kg can be simulated for 1 millisecond (approximately) in the facility. Free stream Mach numbers from 5.75-12 can be generated with a good repeatability (± 5%). Free stream conditions for the present experiments are given in table 1. A representative pitot pressure profile and stagnation pressure profile (at the end of the shock tube) are shown in figure 12 and a schematic diagram of HST2 is shown in figure 13.

Table 1. Free stream conditions for the present experiments

Driver gas	P_0 (kPa)	H_0 (MJ/kg)	M_∞	P_∞ (kPa)	T_∞ (K)	Re_∞ (m^{-1})
N_2	290	0.8	5.75	0.24	100	5.4×10^5
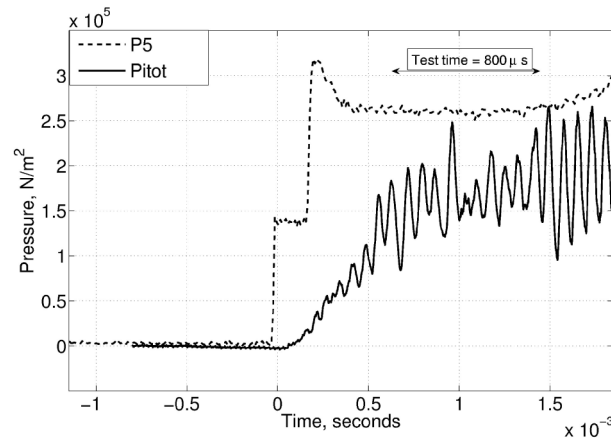
Figure 12.   Superimposed traces of P5 and 10×Pitot
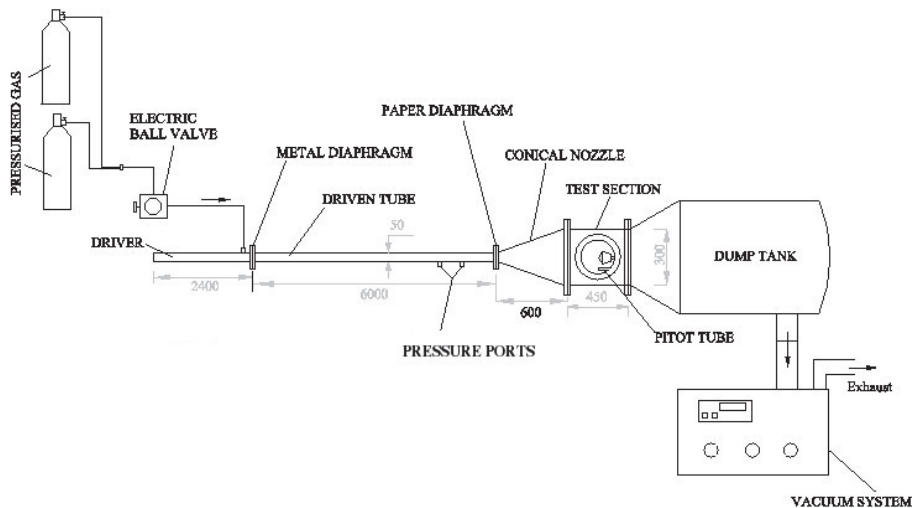
Figure 13.   Schematic diagram of the IISc hypersonic shock tunnel HST 2

3.2. Flat plate geometry

The experiments were carried out on flat plate models. Figure 14 shows a scaled drawing of a flat plate. Plates were with chamfered leading edge. This was to ensure that the shock due to finite thickness of the leading edge did not interfere with the flow. There were two kinds of through holes (4 mm diameter) on the plates, one was perpendicular whereas the other one was inclined at an angle of 45° at a distance of 75 mm from the leading edge and midway in the span-wise direction. A typical flat plate was attached to the bottom of the test section firmly by two thin (2 mm thickness) metallic strips during experiments.

3.3. Injection system

Nitrogen was injected into the oncoming hypersonic cross-flow. The injection was controlled by a fast acting valve (Parker, Kuroda, EJ-15 series). The valve is normally closed when the inlet pressure is above one atmosphere but less than 5 bar. The response time of the valve is 1 millisecond. In other words, it takes 1 millisecond for the valve to open fully after trigger and the pressure reaches a steady value at the outlet of the valve when its inlet is connected to a high pressure reservoir. The valve was triggered by a signal from a pressure transducer mounted on the shock tube 2 m upstream of the nozzle

exit. This was to open the valve shortly ahead of the start of the test flow. The rectangular nature of the signal kept it open longer than the steady test time. During experiments one end of the valve was connected to a high pressure reservoir through a pipe while the other end was connected to the flat plate through a pipe and a conical injector. The valve was mounted inside the test section to minimize the time taken by nitrogen to reach the injection port from the exit of the valve. To determine whether the jet velocity was sonic or not at the port, few experiments were carried out without the hypersonic cross-flow and with the pitot pressure probe mounted 20 mm above the port. The pressure inside the test section was maintained equal to the static pressure of cross-flow during experiments. A photograph (using Schlieren system) of the flow field showed a bow shock ahead of the pitot probe. A representative profile of total jet exit pressure is given in figure 15.
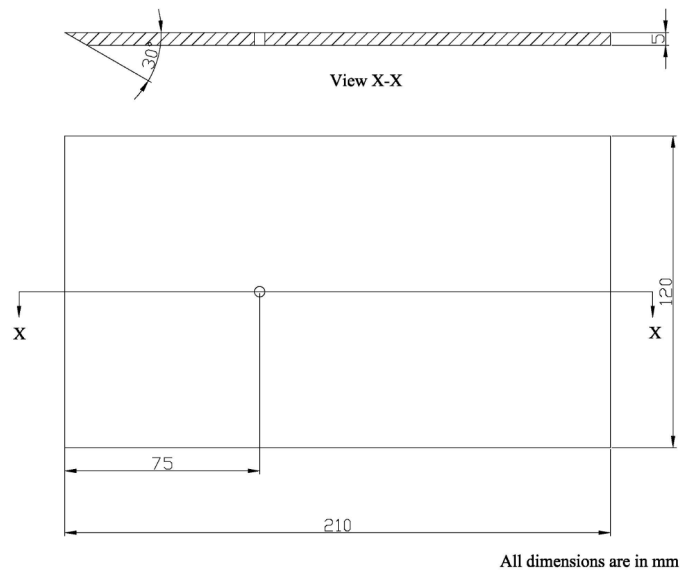
Figure 14.   Scaled drawing of a typical flat plate with circular port
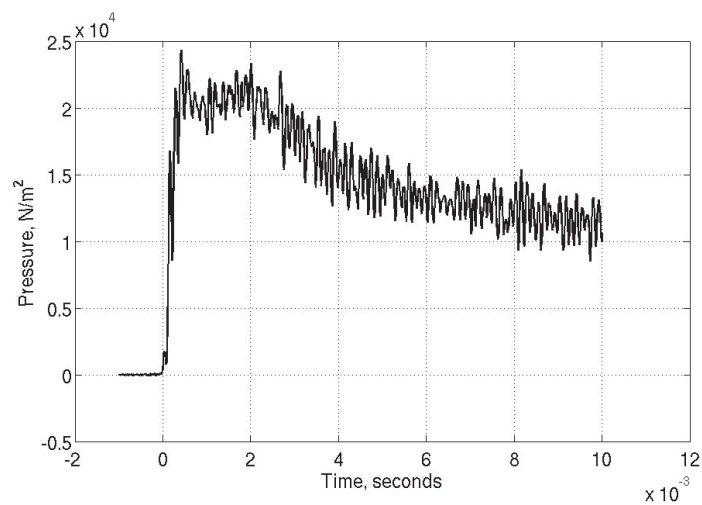
Figure 15.   A Representative total jet pressure profile

3.4. Flow visualization

A 'z-type' Schlieren set up was used for flow field visualization. Details of the Schlieren set up can be found in Satheesh et al. [28]. Two concave mirrors of focal length 96 inches were used to obtain parallel rays of light. A 300 watts North Star lamp with C-Clamp base was used as a continuous light source. A high speed camera (Phantom 7.2, Ms Vision Research, USA) at a resolution of 800×600 mega pixels was used to take sequential snapshots of the flow field. The sample rate and exposure time for different experiments are mentioned at appropriate places.

4. EXPERIMENTAL RESULTS

Several experiments were carried out for both normal and oblique injections. The jet static pressure p_j, total jet pressure P_0, jet Mach number M_j and jet to free stream momentum flux ratio

$$J = (\gamma p M^2)_j / (\gamma p M^2)_\infty$$

are shown in table 2.

Table 2. Conditions for the jet

Condition	P_0 (Pa)	p_j (Pa)	M_j	J
1	1.72×10^5	91083.06	1.0	13.69
2	3.44×10^5	182166.13	1.0	27.38

The aim of flow visualizations was mainly to observe the jet penetration depth into the oncoming cross-flow for normal and oblique injections. Figures 16, 17, 18, 19 show the photographs of the flow field at steady state. Here the steady state refers to the gross state reached by the flow when there is no change in flow feature limited by the camera capacity. The frame interval and exposure are mentioned in the caption of each figure. Identified flow structures for Condition 1 after the flow reaches steady state is given in figure 20.
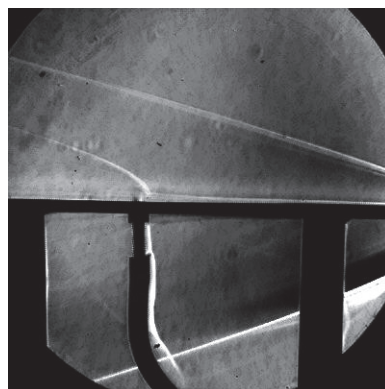
Figure 16.   A photograph of the flow field, condition 1, sample rate 10000 pps, exposure time 98 µs, normal injection
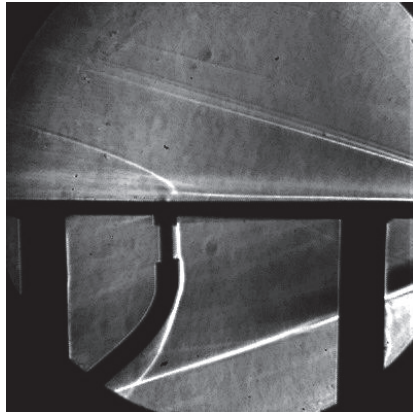
Figure 17.   A photograph of the flow field, condition 2, sample rate 10000 pps, exposure time 98 µs, normal injection
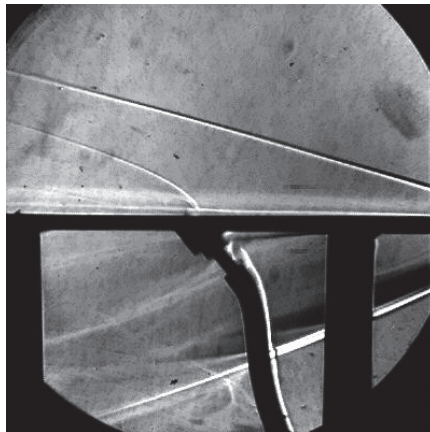
Figure 18.   A photograph of the flow field, condition 1, sample rate 12048 pps, exposure time 77 µs, oblique injection
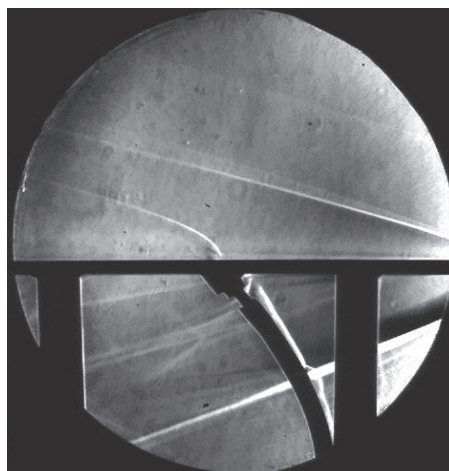
Figure 19.   A photograph of the flow field, condition 2, sample rate 6097 pps, exposure time 156 µs, oblique injection
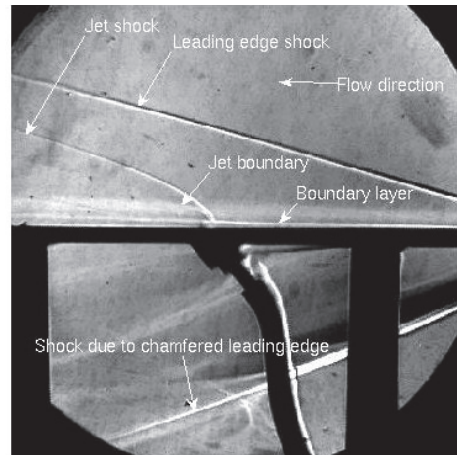
Figure 20.   A photograph of the flow field with identified structures, Condition 1, oblique injection

5. COMPARISON OF JET PENETRATION

The penetration depth of the injected jet into the cross-flow is taken to be the depth of the farthest streamline coming out of the port, which is measured normal to the flat plate. Determination of experimental jet penetration depth was based on measurements on the images which were taken during experiments. The density of the injected jet is two orders of magnitude higher than that of the free-stream. So the jet boundary in the cross-flow was identifiable in the schlieren images up to certain distance down-stream of the port. Movies of duration of the total test time were made and in those the identification of jet boundary was easier than still images. Additionally it is possible to have a closer look into a particular area by zooming in, which is one of the good features of the camera control software. In the camera control software it is possible to assign physical distance between two points in an image. Then the software gives distance between any two points on an image which is equal to the physical distance. Following the above procedure the jet penetration depth was measured and non-dimensionalized by the port diameter. For elliptic port, an effective diameter of $(4 \times \text{area}/\pi)^{1/2}$ was used. Figure 18 shows the plot of jet penetration depth normal to the flat plate for different experimental conditions. The flow direction is from right to left. Penetration depth is more in case of normal injection than oblique injection for the same momentum flux ratios. However, there is little difference in the penetration depth for the two momentum flux ratios for the same type of injection (i.e. normal or oblique). Jet penetration depths determined from 3D numerical simulation are shown in figure 19. For this a slice was taken midway in the span-wise direction of the 3D domain and the streamlines only from the port were plotted to determine the distance of the farthest streamline normal to the plate. Numerical simulations predicted less penetration depth than experiments for normal injection. However for oblique injection the predictions were very close to that obtained from experiments.

6. CONCLUSIONS

Jet penetration depth in a hypersonic cross-flow is found to be a weak function of jet to free-stream momentum flux ratio (J). This is borne out by very little increase in penetration depth when J is doubled for the same type of injection. The penetration depth is higher for normal injection than oblique injection for same jet to free-stream momentum flux ratio. This is because of the lower magnitude of the normal velocity component for oblique injection. The stagnation pressure loss is also higher for normal injection than oblique injection. However, the jet streamlines spread wider for oblique injection than normal injection as shown in figure 5 and 6 and this may be similar to the axis switching phenomenon observed in subsonic jets. This is favourable from the point of view of mixing. Also in case of oblique injection increase in momentum flux results in more span-wise spreading of the injected jet.

(a)

(b)

(c)

(d)
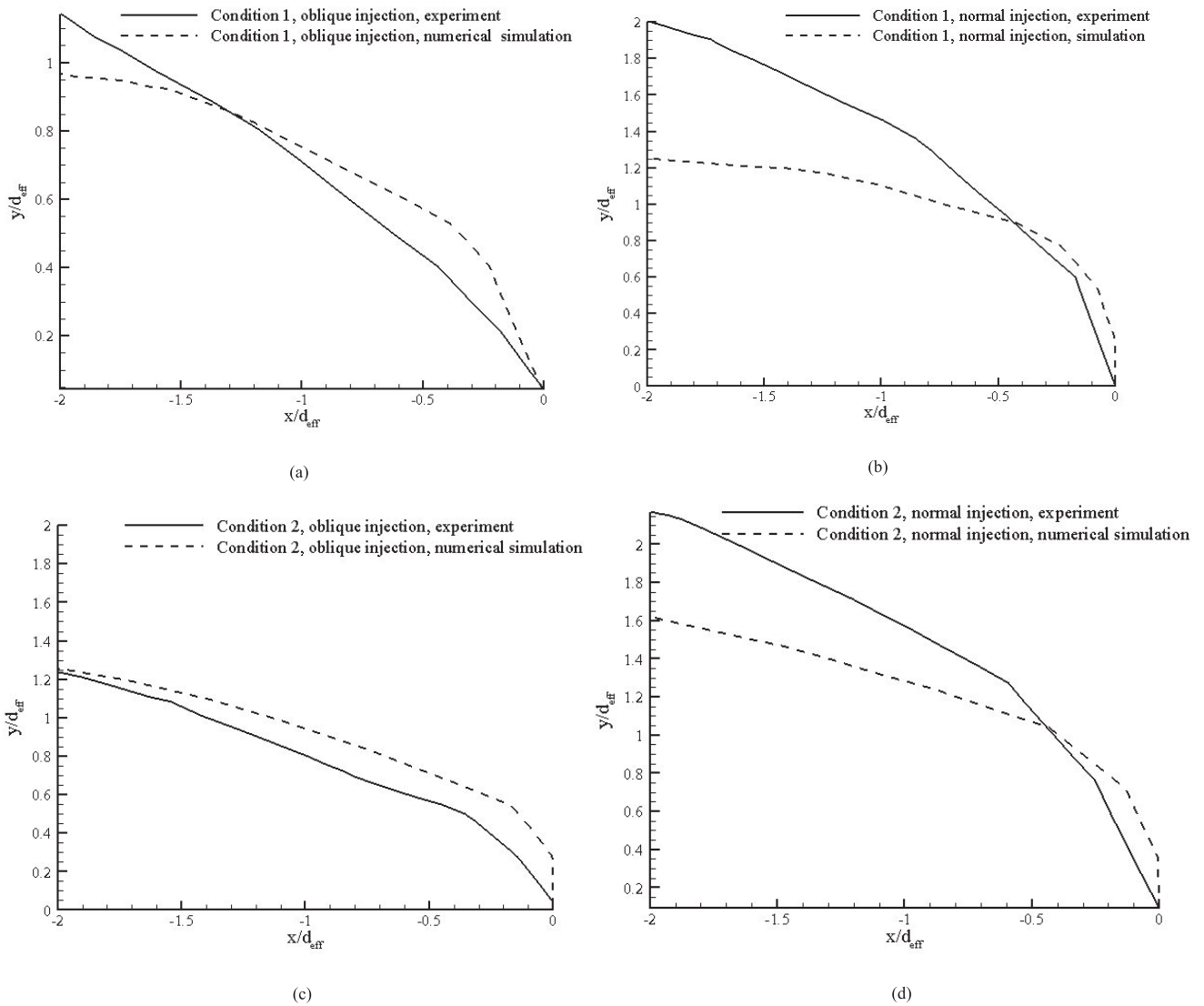
Figure 21.   Comparison of jet penetration depth for normal and oblique injections

In view of the above observations it may be concluded that the momentum flux ratio should not be raised too much to achieve high penetration depth. Rather the height of the combustion chamber should be reduced to operate efficiently. Oblique injection (elliptic port) should be preferred over a normal one for better fuel spreading and hence mixing.

REFERENCES

[1]   J. R. McGuire, R. R. Boyce and N. R. Mudford, *Radical-Farm ignition Processes in Two-Dimensional Supersonic Combustion*, Journal of Propulsion and Power, Vol. 24, No. 6, 2008, 1248-1257.

[2   Griffin Y. Anderson, Patricia G. Reagon, Paul B. Gooderum, and Roger Russin, *EXPERIMENTAL INVESTIGATION OF A SWEPT-STRUT FUEL INJECTOR CONCEPT FOR SCRAMJET APPLICATION*, NASA TN D-8454, August, 1977.

[3]   Joseph A. Schetz and F. S. Billig, *Penetration of gaseous jets injected into a supersonic stream*, Journal of Spacecrafts and Rockets, 3, 1966, 1658–1665.

[4]   F. S. Billig, R. C. Orth, and M. Lasky, *A unified analysis of gaseous jet penetration*, AIAA Journal, Vol. 9, 1971, 1048–1058.

[5]   F. W. Spaid and E. E. Zukoski, *A study of the interaction of gaseous jets from transverse slots with supersonic external flows*, AIAA Journal, Vol. 6, 1968, 205–212

[6]   S. Aso, S. Okuyama, Y. Ando, and T. Fujimori, *Two-dimensional and three dimensional mixing flow fields in supersonic flow induced by injected secondary flows through transverse slot and circular nozzle*, AIAA Paper, *31st* Aerospace Sciences Meeting & Exhibit, Reno, NV, 93-0489, 1993.

[7]   M. R. Gruber, A. S. Nejad, T. H. Chen, and J. C. Dutton, *Mixing and penetration studies of sonic jets in a mach 2 free-stream*, Journal of Propulsion and Power, Vol. 11, 1995, 315–323.

[8]   J. G. Santiago and J. C. Dutton, *Crossflow vortices of a jet injected into a supersonic cross-flow*, AIAA Journal, Vol. 35, 1997, 915–917.

[9]   D. E. Everett, M. A. Woodmansee, J. C. Dutton, and M. J. Morris, *Wall pressure measurements for a sonic jet injected transversely into a supersonic cross-flow*, Journal of Propulsion and Power, Vol. 14, 1998, 861–868.

[10] A. Ben-Yakar, M. G. Mungal, and R. K. Hanson, *Time evolution and mixing characteristics of hydrogen and ethylene transverse jets in supersonic cross-flows*, Physics of Fluids, 18(026101), 2006.

[11] D. P. Rizzetta, *Numerical simulation of slot injection into a turbulent supersonic stream*, AIAA Journal, Vol. 30, 1992, 2434–2439.

[12] S. Aso, S. Okuyama, M. Kawai, and Y. Ando, *Experimental study of mixing phenomena in supersonic flow with slot injection*, AIAA Paper, 29th Aerospace Sciences Meeting, Reno, NV, 91-0016, 1991.

[13] F. Grasso and V. Magi, *Simulation of transverse gas injection in turbulent supersonic air flows*, AIAA Journal, 33, 1995, 56–62.

[14] P. Gerlinger, J. Algermissen, and D. Bruggemann, *Numerical simulation of mixing for turbulent slot injection*, AIAA Journal, Vol. 34, 1996, 73–78.

[15] R. Dhinagaran and T. K. Bose, *Numerical simulation of two-dimensional transverse gas injection into supersonic external flows*, AIAA Journal, Vol. 36, 1998, 486–488.

[16] David C. Wilcox, *Reassessment of the scale-determining equation for advanced turbulence models*, AIAA Journal, Vol. 26, 1988, 1299–1310.

[17] Ratan Joarder and G. Jagadeesh, *Roe linearization for the Euler equations augmented by the convective terms from the k-ε turbulence model*, International Journal for Numerical Methods in Fluids, Vol. 57, 2008, 1569–1576.

[18] P. L. Roe, *Approximate riemann solvers, parameter vectors, and difference schemes*, Journal of Computational Physics, Vol. 43, 1981, 321–326.

[19] B. Van Leer, *Towards the ultimate conservative difference scheme.v.a second-order sequel to Godunov's method*, Journal of Computational Physics, Vol. 32, 1979, 101–136.

[20] G. D. Van Albada, B. Van Leer, and W. W. Roberts, *A comparative study of computational methods in cosmic gas dynamics*, Astron. Astrophys., Vol. 108, 1982, 76–84.

[21] R. Peyret and T. D. Taylor, *Computational Methods for Fluid Flow,* Springer, Berlin, 1983.

[22] S. Sarkar, G. Erlebacher, M. Y. Hussaini, and H. O. Kreiss, "*The analysis and modeling of dialational terms in compressible turbulence*", CR-181959, *NASA*, 1989.

[23] R. A. Thomas, Bussing, and Earll M. Murman, *Finite-volume method for the calculation of compressible chemically reacting flows*, AIAA Journal, Vol. 26, 1987, 1070–1078.

[24] K. G. Powell and B. Van Leer, *Tailoring explicit time marching schemes to improve convergence characteristics*, *Computational Fluid Dynamics VKI*, Vol. 2, 1990, 30–42.

[25] D. A. Anderson, J. C. Tannehil, and R. H. Pletcher, *Computational Fluid Mechanics and Heat Transfer*, 2nd edition. Taylor and Francis, Philadelphia, 1997.

[26] V. Wheatley and P. A. Jacobs, *Fuel Injection via Rectangular Cross-section Injectors for Mixing enhancement in Scramjets*, 17th Australasian Fluid Mechanics Conference, Auckland, New Zealand, 5-9 December, 2010.

[27] Holden M., Bower D. and Chadwick K, "*Measurements of Boundary-Layer transition on Cones at Angle of Attack for Mach Numbers from 11 to 13*", AIAA Paper 95-2294, June 1995.

[28] K. Satheesh, G. Jagadeesh, and K. P. J. Reddy, *High speed schlieren facility for visualization of flow fields in hypersonic shock tunnels*, Current Science, Vol. 92, 2007, 56–60.